

## DIGITAL TERRAIN MODELING USING FINITE ELEMENT METHODS MESHLESS

Gustavo R. Scandolieri<sup>1</sup>, Danillo R. Pereira<sup>1\*</sup>, Francisco A. Silva<sup>1</sup>,  
Leandro L. Almeida<sup>1</sup>, Helton M. Sapia<sup>1</sup> and João F. C. Silva<sup>2</sup>

<sup>1</sup>*Department of Computer Science, University of Western São Paulo (Unoeste), Presidente Prudente,  
São Paulo, Brazil*

<sup>2</sup>*Department of Cartography, Faculty of Science and Technology, São Paulo State University (Unesp),  
Presidente Prudente, São Paulo, Brazil*

Received 12 December 2017; received in revised form 1 July 2018; accepted 03 July 2018

---

**Abstract:**

Digital Terrain Modeling (DTM) is a computational model of the earth surface that represents relief and it has a wide range of applications. This work proposes a new approach to DTM using the Finite Element Method (FEM) point-based instead of mesh-based. The points used by the proposed methodology were obtained by data captured by satellite images. The most methods require the precomputation of a mesh on the surface of the terrain. Our methodology overcomes the mesh step, and then the modeling process is very fast.

**Keywords:** Digital Terrain Model, Finite Element Method

© 2018 Journal of Urban and Environmental Engineering (JUEE). All rights reserved.

---

\* Correspondence to: Danillo R. Pereira, Tel.: +55 18 3229 1060.  
E-mail: [danilopereira@unoeste.br](mailto:danilopereira@unoeste.br)



## INTRODUCTION

Digital Terrain Model (DTM) is a topographic mathematical model of the earth surface that represents relief's variations and can be manipulated by computational methods (Barnhill, 1977). Thus DTM represents the terrain elevations over the surface to being analyzed. To perform this task is necessary capturing spot samples on the interest region surface (Ochi *et al.*, 2006; Zanardi, 2006; Felgueiras, 1997). The use of DTM is widely used in several areas of knowledge, mainly in engineering, providing very important kinds of information, for example: in the feasibility of urban planning (road construction projects, tunnels, dams and respective land displacements); in the extraction of drainage levels and networks; in research and environmental impact studies and etc. (Piteri *et al.*, 2007). In addition, DTM is a very powerful tool to solving problems of project deployments, aiding to perform volume calculations, areas and generate maps (Sangreman *et al.*, 2014).

There are several techniques to obtain the DTM, among them are: cartographic, topographic survey and photogrammetry. Generally, samples obtained by aerial-photogrammetric surveys are used. This work is performed by airplanes equipped with photographic cameras and metric sensors that calculate the altitude of the sampled land, as shown in Fig. 1.

The data obtained by the aerial photogrammetric can be interpreted as a set of points  $(x_i, y_i)$  in two-dimensional space (2D). Each point  $(x_i, y_i)$  of this space has associated a third value ( $z_i$ ) which denotes the point altitude (elevation). So you can define two sets of sampling points, they are: (i)  $P = \{(x_0, y_0), (x_1, y_1), \dots, (x_{n-1}, y_{n-1})\}$  e (ii)  $S = \{(x_0, y_0, z_0), (x_1, y_1, z_1), \dots, (x_{n-1}, y_{n-1}, z_{n-1})\}$ ; where  $n$  denotes the number of points sampled. A two-dimensional example of the set  $P$  of sampled points can be seen in Fig. 2.

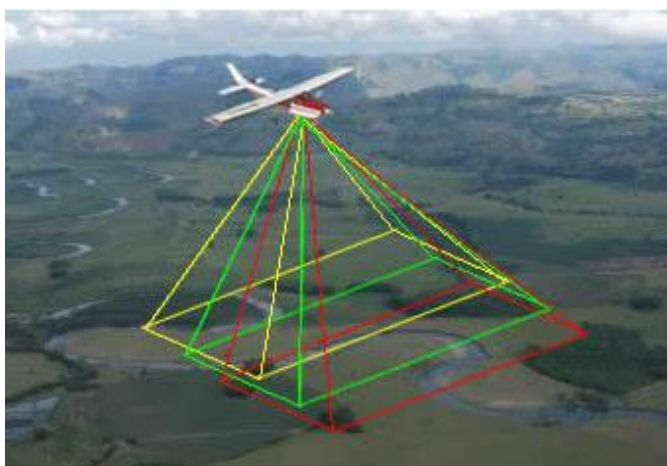


**Fig. 1** Illustration of the process of acquisition of the terrain data using aerial photogrammetric.

Source: <http://www.ipssurvey.com/foto1.jpg>

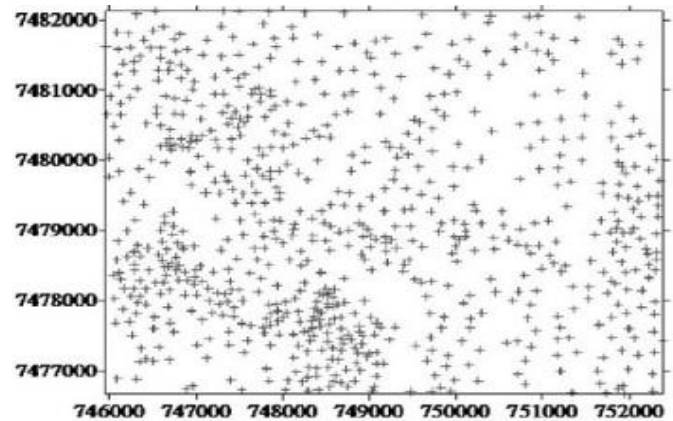


**Fig. 2** Illustration of the set of points  $P$  sampled.

In general, the value of  $z_i$  is obtained using a distance sensor that emits a wave, and by the delay time of its reflection is computed the estimated altitude (distance). In this way it is possible to obtain the deformation of the terrain over the sampled points.

Traditional methods of DTM require a priori the polygonal mesh generation (usually triangular or quadrangular) on the convex hull of the points sampled (set  $P$ ). The reconstruction of a terrain model by DTM using triangulation of points is not a very recent idea. The main advantage of triangular meshes is the ability to make changes in the resolution of the model according to its complexity, providing an adaptive behavior (Bakambu *et al.*, 2006; Lawson, 1977). The use of triangular meshes has been widely used in the various terrain modeling applications, in order to reduce geometric information, mainly in aerial photogrammetry (Fayek & Wong, 1996). However it's worth highlighting that computational cost for generating the mesh is considerable (Edelsbrunner, 2001).

Triangular mesh do not have a unique triangulation algorithm, it has several different solutions. The most used algorithm in triangulation is Delaunay (Watson, 1981) that it is able to maximize the lowest angle of each mesh triangle, so this method allows a triangle mesh with elements more regular (Sibson, 1978; Itame, 2001).

The redefinition of the mesh in its evolution process generates problems in a way to coincide with the discontinuities, this ends up generating a great degradation of the precision of the results and making the process much slower (Belytschko *et al.*, 1996).

The quality of the model is directly related to the amount of data sampled, in applications where realism is desired, a very high number of sampled points must be possessed; that is, the greater the number of interpolations made in the generation of the model the higher the quality of the model (Barros, 2002).

This work proposes a novel DTM method meshless only using the sampled points using Finite Element Method (FEM) (Giacchini, 2012). Due the method be meshless the computational cost is considerably reduced when compared with DTM traditional methods that use meshes. We too analyze the precision of the proposed methods using ground-truth models. The main idea of this work is not to compare results but rather to propose an unprecedented, very fast and very promising methodology. In this way the goal of the work is propose a new solution and to contribute with another researchers of the DTM area.

The remaining of the paper is organized as follows: Section 2 presents the Finite Element theoretical background. The methodology is described in the Section 3. The Section 4 presents the results and analysis. Conclusion is discussed in Section 5.

## 2 FINITE ELEMENT METHODS (FEM)

The FEM is a useful mathematical tool for applications that require approximation or interpolation. It is a numerical method widely used to obtain approximations of mathematical problems that generally originate from a physical model. The efficiency of the FEM is related to an initial phase of preprocessing. This preprocessing is related with domain division of the object at the geometric and topological level, decomposing a complex domain into a mesh of elements, such as triangles, quadrilaterals (or even formed by both types of elements). This phase is of extreme importance for the regularity and positioning of the elements of the mesh, since they will determine the quality of the approximate solution, directly influencing the graphical representation of the model (Pereira, 2006).

However, very recently Pereira (2017) proposed the FEMaR, a regression machine based in FEM meshless. Based in Pereira, we propose a novel meshless DTM technique that is very accurate and fast.

### Approximation Bases

Let a vector space  $W$  composed of  $\varphi_1, \varphi_2, \dots, \varphi_n$  where each  $\varphi$  elements is linearly independent and any elements of  $w \in W$  can be obtained by follow linear combination:

$$w = \sum_{i=1}^n a_i \varphi_i \tag{1}$$

where  $a_1, a_2, \dots, a_n$  are the coefficients and  $\varphi = (\varphi_1, \varphi_2, \dots, \varphi_n)$  is a base of  $W$  (Pereira, 2017).

### Interpolation

Given  $n$  points  $x_1, x_2, \dots, x_n$  of the domain  $W$  and  $n$  associated values  $y_1, y_2, \dots, y_n$  of the space  $V$ . The

interpolation aims to find a function  $B \in A$  that interpolates the pairs  $(x_i, y_i)$ , thus:

$$B(x_i) = y_i \text{ for all } i. \tag{2}$$

The space  $A$  is composed by  $\varphi = (\varphi_1, \varphi_2, \dots, \varphi_n)$ , and needs of the values  $a_1, a_2, \dots, a_n$  in the way that  $\sum_{i=1}^n a_i \varphi_i(x_j) = y_j$  for all  $j$ .

In the context of DTM, given the points sampled, the interpolation is necessary to increase the number of points that represent the model, mainly in regions where the points were not sampled (sub-sampled regions), improving the model representation quality (Barbosa, 1999). It is very important to note that the sampling point  $x$  can be found in any  $R^m$ .

### 2.3 Shepard Basis

For the Shepard basis (Shepard, 1968) each element  $\varphi_i$  is denoted by the Eq. 3.

$$\varphi_i(x) = \frac{w(x, x_i)}{\sum_{j=1}^n w(x, x_j)} \tag{3}$$

$W$  is a non-negative function, so that  $w(x, x_i)$  tends to go to infinity when  $x$  tends to  $x_i$ . A very common function used by Shepard is presented in Eq. 4 ( $k \geq 0$ ) (Pereira, 2009).

$$w(x, x_i) = \frac{1}{|x - x_i|^k} \tag{4}$$

Figure 3 shows the behavior of the Shepard basis using different values of  $k$ .

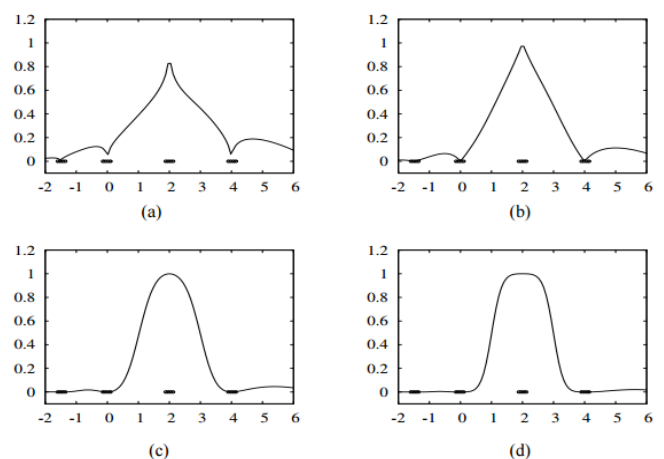


Fig. 3 An element of the Shepard base with different values of  $k$  for the points  $x_i$  indicated on the horizontal axis. (a)  $k = 0.5$  (b)  $k = 1$  (c)  $k = 2$  (d)  $k = 3$  (Pereira, 2009).

**Interpolation**

The normalized radial basis has a unique mother function, which uses the distance from point  $x$  to point  $x_i$  of a set of finite points  $x_1, x_2 \dots, x_n$ , the formula being:

$$\varphi_i(x) = \Psi(|x, x_i|) \tag{5}$$

where  $|x, x_i|$  denotes the Euclidean distance between  $x$  e  $x_i$ . The mother function used is Gaussian bell, it is:

$$\Psi(r) = \exp\left(-\frac{1}{2}\left(\frac{r^2}{r^0}\right)\right) \tag{6}$$

Some radial normalized basis can be seen in Fig. 4.

The very same function interpolated by a Shepard bases and radial normalized bases can be seen in Fig. 5 (Pereira, 2009).

**METHODOLOGY**

Our proposed methodology is able to interpolate the terrain surface and the pixel color of each sub-sampled region. So, besides the terrain model, our methodology to create a graphical 3d model, given an image very realistic. The schematic diagram of the proposed approach can be seen in Fig. 6. Given a dataset of discrete sampled data under terrain surface our methodology split the data information in three groups, they are: (i) position, (ii) height, and (iii) texture. In the sequence, we computed the interpolation weights and then we interpolated the no sampled point information (height and texture).

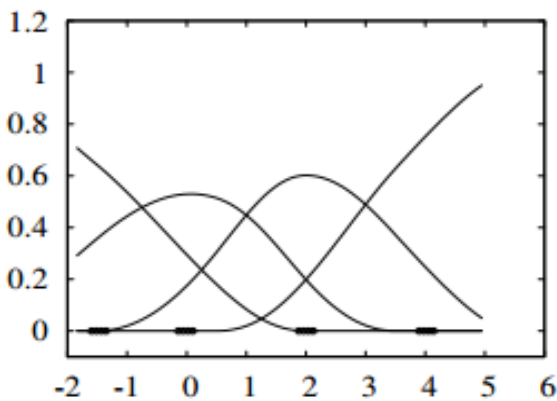


Fig. 4 Elements of normalized radial base for the points  $x_i$  indicated on the horizontal axis (Pereira, 2009).

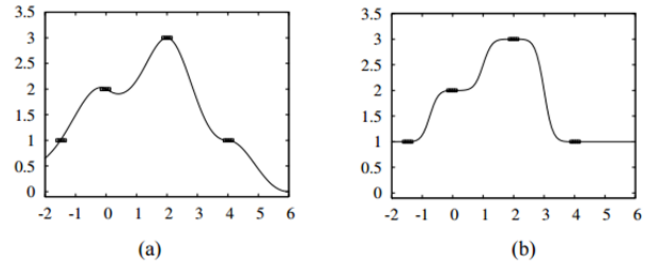


Fig. 5 Illustration of the interpolation result using (a) normalized radial base and (b) Shepard base with  $k = 2$  (Pereira, 2007).

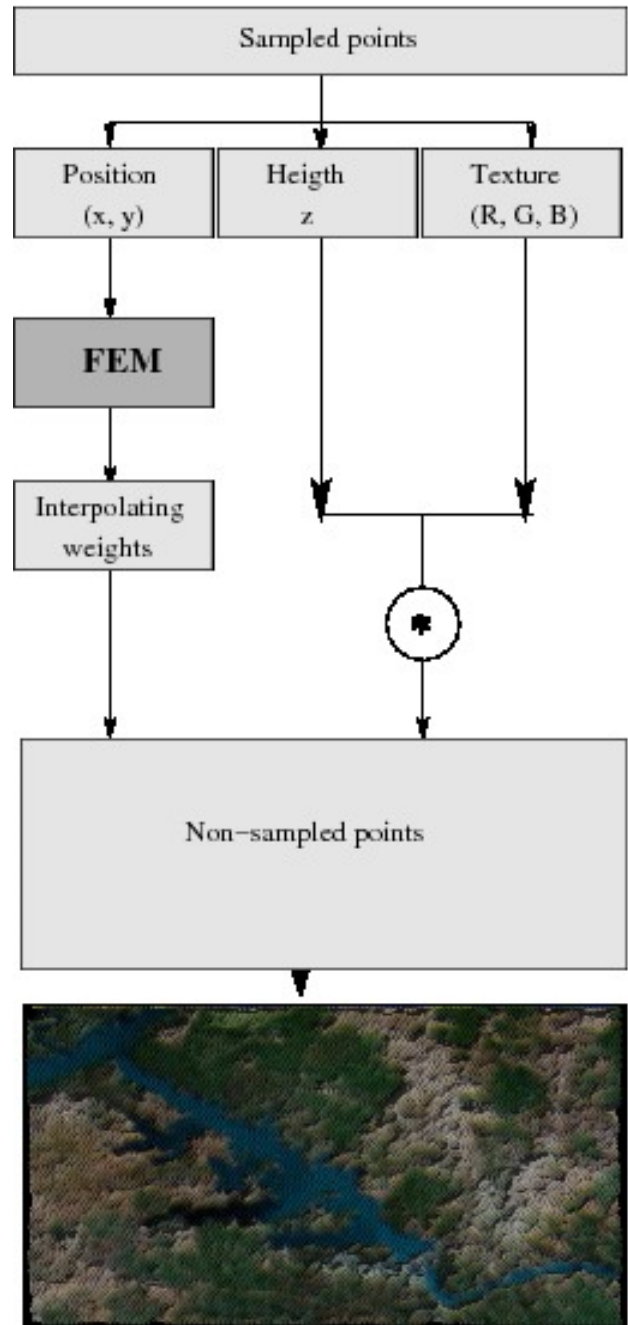


Fig. 6 Schematic diagram of the proposed method.

In our experiments, we used four images, three real images and one synthetic (Fig. 7). To facilitate to the reader we denote the images as **dataset1**, **dataset2**, **dataset3**, and **synthetic dataset**, respectively.



Fig. 7 Images used in the experiments.

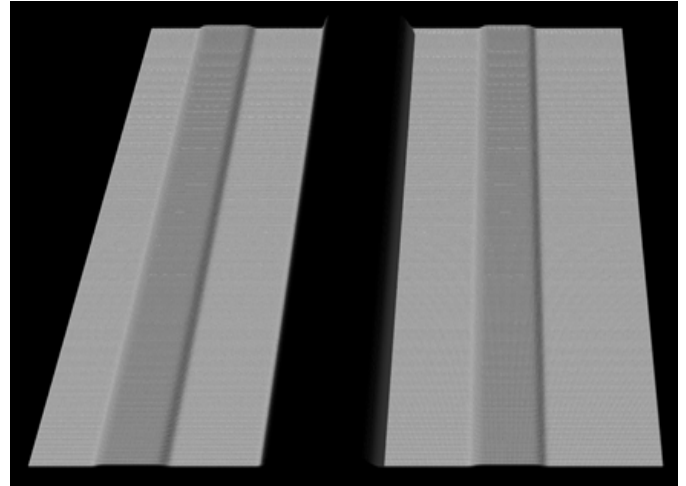


Fig. 8 Interpolated synthetic image with radial base normalized in grayscale to demonstrate the definition of height of the Z axis where is possible identify the 3D surface details.

Due the images not contains surface information to perform the modeling of the terrain, we were transformed into gray scales to determine the model reliefs that is determined the Z axis (Fig. 8). It is not possible to determine the altitude of an image, due to the fact of the image to be 2D, having only two coordinates ( $x, y$ ), and the model to be generated is 3D, having three coordinates ( $x, y, z$ ). So, we considered that lighter the pixel in grayscale the higher its altitude.

In the sequence to obtain the relief Z point, the FEM was used with two different bases of interpolation, they are: (i) normalized radial base, and (ii) the Shepard base. For each image, we consider the two different spacing between pixels: (i) two by two, and (ii) four by four.

In addition to the interpolation of the surface relief, we also interpolated the texture considering the RGB pixel values from sampled points. In this context, the surface and texture are linearly interpolated, so the complexity of the interpolation process is  $O(n)$ . It is important highlighted that the weights from Eq. 3 or Eq. 6 are computed one once time for texture and relief.

## RESULTS

To visualize the digital terrain reconstructed we used a very popular ray tracing tool called POV-RAY (available in <http://www.povray.org>), where the interpolation information (relief and texture) are passed through of a script that read the contents of the files and generated the images.

The digital terrain model of the synthetic dataset can be seen in Fig. 8 where is possible note clearly the 3D effect generated by our methodology. The digital model of the **dataset1** can be seen in Fig. 9 and Fig. 10. The Fig. 9 and Fig. 10 present the results of the digital terrain considering the normalized radial basis using



**Fig. 9** Digital terrain model of the **dataset1** using radial basis and spacing of two by two.



**Fig. 11** Digital terrain model of the **dataset2** using radial basis and spacing of two by two.



**Fig. 10** Digital terrain model of the **dataset1** using radial basis and spacing of four by four.



**Fig. 12** Digital terrain model of the **dataset2** using radial basis and spacing of four by four.

spacing of two by two and four by four, respectively. In other way, the **Fig. 15** and **Fig. 16** present the digital terrain model considering Shepard basis using spacing of two by two and four by four, respectively.

The digital model of the **dataset2** can be seen in **Fig. 11**, **Fig. 12** and **Fig. 17**, **Fig. 18**. **Figure 11** and **Fig. 12** present the results of the digital terrain considering the normalized radial basis using spacing of two by two and four by four, respectively. In other way, the **Fig. 17** and **Fig. 18** present the digital terrain model considering Shepard basis using spacing of two by two and four by four, respectively.

The digital model of the **dataset3** can be seen in **Figs 13–20**. **Figures 13–14** present the results of the digital terrain considering the normalized radial basis using spacing of two by two and four by four, respectively. In other way, the **Figs 19–20** present the digital terrain model considering Shepard basis using spacing of two by two and four by four, respectively.



**Fig. 13** Digital terrain model of the **dataset3** using radial basis and spacing of two by two.



**Fig. 14** Digital terrain model of the **dataset3** using radial basis and spacing of four by four.

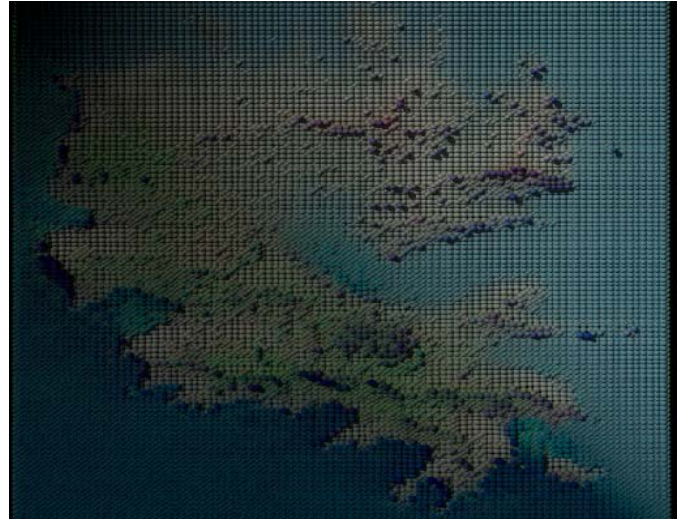


**Fig. 17** Digital terrain model of the **dataset2** using Shepard basis and spacing of two by two.

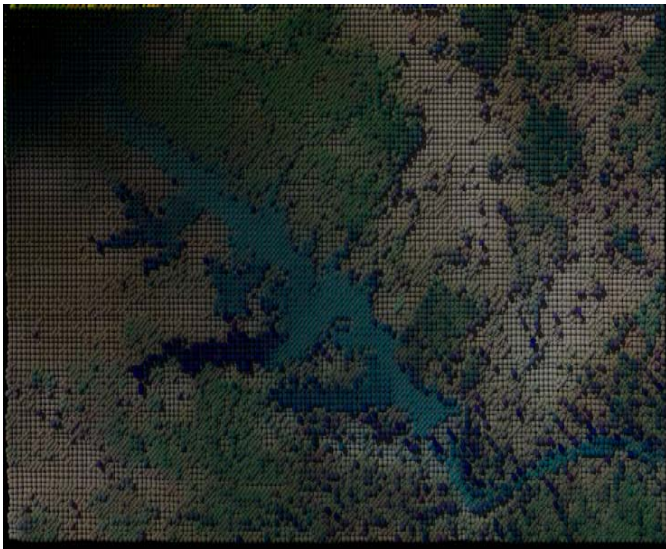


**Fig. 15** Digital terrain model of the **dataset1** using Shepard basis and spacing of two by two.



**Fig. 18** Digital terrain model of the **dataset2** using Shepard basis and spacing of four by four.



**Fig. 16** Digital terrain model of the **dataset1** using Shepard basis and spacing of four by four.



**Fig. 19** Digital terrain model of the **dataset3** using Shepard basis and spacing of two by two.

Clearly, it is possible to observe that the results obtained by the radial basis are visually much better than those of the Shepard basis, mainly due the non-smooth behavior of the Shepard basis (**Fig. 5**).

The influence of the spacing is more visible in Shepard basis, however too degenerate the Radial basis, as expected. In order to perform a more precise and analytical comparison between the both types of bases we used the well-known metrics Mean Absolute Error (MAE) and Mean Squared Error (MSE) considering the Z value obtained. The computer used for experiments has 8GB of RAM and i5 6500 processor.



**Fig. 20** Digital terrain model of the dataset3 using Shepard basis and spacing of four by four.

**Table 1.** Comparison metrics for the dataset1 using Shepard and Radial basis.

Dataset		dataset1			
Spacing		2		4	
Shepard	Fig	Fig. 15	Fig	Fig. 16	
	MAE	80.421124	MAE	81.396648	
	MSE	9035.863866	MSE	9192506332	
	Time	11.00 min	Time	11.01 min	
Normalized Radial	Fig	Fig. 9	Fig	Fig. 10	
	MAE	79.994168	MAE	80.004225	
	MSE	8971.539481	MSE	8973.539941	
	Time	13.00 min	Time	14.00 min	

**Table 2.** Comparison metrics for the dataset2 using Shepard and Radial basis.

Dataset		dataset2			
Spacing		2		4	
Shepard	Fig	Fig. 17	Fig	Fig. 18	
	MAE	96.910022	MAE	98.186888	
	MSE	12830.362712	MSE	13067.795555	
	Time	09.35 min	Time	09.16 min	
Normalized Radial	Fig	Fig. 11	Fig	Fig. 12	
	MAE	96.299058	MAE	96.307562	
	MSE	12705.898069	MSE	12707.578089	
	Time	11.85 min	Time	10.46 min	

**Table 3.** Comparison metrics for the dataset3 using Shepard and Radial basis.

Dataset		dataset1			
Spacing		2		4	
Shepard	Fig	Fig. 19	Fig	Fig. 20	
	MAE	73.809473	MAE	74.683891	
	MSE	7446.869099	MSE	7578.048903	
	Time	12.54 min	Time	12.34 min	
Normalized Radial	Fig	Fig. 13	Fig	Fig. 14	
	MAE	73.429301	MAE	73.415194	
	MSE	7391.531702	MSE	7389.497806	
	Time	13.68 min	Time	13.33 min	

**Tables 1–3** present the comparison metrics considering dataset1, dataset2 and dataset3 with processing time, MSE and MAE. In all experiments, the Radial basis obtained better results than Shepard, however the Shepard is faster than Radial basis. The better results obtained by Radial basis is due the smooth behavior of the basis (**Fig. 5a**), in other hand; Shepard basis contains some slopes regions (**Fig. 5b**). The Radial is slower than Shepard basis due the computation of the exponential function (see **Eq. 6**). Both basis obtained very promising results and generated very realist images without the need of mesh generation.

## CONCLUSIONS

The main idea of this work is not to compare results but rather to propose an unprecedented, very fast and very promising methodology. The results obtained through tests performed we can concluded that the Shepard base although faster to process does not have a so good representation of the model, and its altitude error and RGB ends up being larger than that of the normalized radial base. Since the normalized radial base method presents a great appearance, representing the model, having an altitude error and RGB slightly lower than the base of Shepard but a slightly higher processing time as well. The results presented are very promising; the normalized radial basis can represents precisely the 3D terrain models. The size of the image does not influence the quality of the model, but rather the amount of interpolated elements. It is worth noting that there are no DTM designs in the literature that use finite element methods without the use of a mesh to generate the model.

## REFERENCES

- Barbosa, R.L. (1999) Geração de Modelo Digital do Terreno por aproximações sucessivas utilizando câmaras digitais de pequeno formato. Master's Thesis, São Paulo State University (Unesp), Brazil.
- Belytschko, T.; Krongauz, Y.; Organ, D.; Fleming, M. & Krysl, P. (1996) Meshless Methods: An Overview and Recent

- Developments. *Computer Methods in Applied Mechanics and Engineering*, 1-4(139), 3–47.
- Bakambu, J.N.; Allard, P. & Dupuis, E. (2006) 3d terrain modeling for rover localization and navigation. In: *The 3rd Canadian Conference on Computer and Robot Vision*, IEEE, 61–61.
- Barnhill, R.E. (1977) Representation and approximation of surfaces. *Proc. of a Symposium Conducted by the Mathematics Research Center, the University of Wisconsin–Madison*. 69–120.
- Barros, F.B. (2002) Métodos sem Malha e método dos Elementos Finitos Generalizados em Análise Não-Linear de Estruturas. Phd Thesis, University of São Paulo, São Carlos.
- Shepard, D. (1968) A two-dimensional interpolation function for irregularly-spaced data. *Proc. of the 23rd ACM national conference*, 517–524.
- Edelsbrunner, H. (2001) *Geometry and Topology for Mesh Generation*. Cambridge Monographs on Applied and Computational Mathematics.
- Felgueiras, C.A. (1997) Análises sobre Modelos Digitais de Terreno em Ambiente de Sistemas de Informação Geográfica. In: *VIII Simpósio Latinoamericano de Percepción Remota y Sistemas de Información Espacial*. Mérida, Venezuela.
- Fayek, R. & Wong, A. (1996) Using hypergraph knowledge representation for natural terrain robot navigation and path planning. In: *International conference on Robotics and Automation*, IEEE, 4, 3625–3630.
- Giacchini, B.L. (2012) Uma Breve Introdução ao Método dos Elementos Finitos.
- Itame, O.Y. (2001) Controle de Qualidade Aplicado na Modelagem Digital de Terreno. Master's Thesis, São Paulo State University (Unesp), Brazil.
- Lawson, C.L. (1977) Software for C1 surfaces interpolation. J. Rice, Academic Press.
- Ochi, V.T.; Françoso, M.T. & Albuquerque, P.J.R. (2006) Mapeamento do Subsolo Utilizando Técnicas de Modelagem Digital de Terreno do Campus da Unicamp – Campinas – Brasil. In: *10º Congresso Nacional de Geotecnia*, 2006, Lisboa. 283–292.
- Pereira, D.R. (2006) Refinamentos Adaptativos Bidimensionais de Delaunay. Monograph of college in Computer Science, São Paulo State University (Unesp), Brazil.
- Pereira, D.R. (2009) Representação e Cálculo Eficiente da Iluminação Global na Síntese de Imagens. Master's Thesis, Institute of Computing, University of Campinas.
- Pereira, D. R. and Papa, J. P. and de Souza, A. N. (2017) FEMaR: A finite element machine for regression problems. *Proc. of International Joint Conference on Neural Networks (IJCNN)*.
- Piteri, M.A.; Meneguete, M.; Santos, A.D. & Oliveira, F.D. (2007). Triangulação de delaunay e o princípio de inserção randomizado. In: *II Simpósio Brasileiro de Geomática*, 655–663.
- Sibson, R. (1978) Locally equiangular triangulations. *The Computer J.* 21(3): 243–245.
- Sangreman, A.P.; Freitas, G. & Costa R.R. (2014) Modelagem De Terrenos Naturais Atraves de Malhas de Triângulos. *Proc. of Series of the Brazilian Society of Computational and Applied Mathematics*.
- Watson, D. (1981) Computing the n-dimensional Delaunay tessellation with application to Voronoi polytopes. *Computer Journal*, v.24, n.2, 167–172.
- Zanardi, R.P. (2006) Geração de Modelo Digital de Terreno a partir de par Estereoscópico do Sensor CCD do Satélite CBERS-2 e Controle de Qualidade das Informações Altimétricas. Master's Thesis, Federal University of Rio Grande do Sul, Porto Alegre.